Pergamon

Atmospheric Environment Vol. 30, No. 16, pp. 2821–2829, 1996

1352-2310/96 $15.00 + 0.00

1352-2310(95)00406-8

A LAGRANGIAN STUDY OF PARTICLE DISPERSION IN THE UNSTABLE BOUNDARY LAYER

G. QUERZOLI

Department of Mechanics and Aeronautics, University of Rome "La Sapienza", Via Eudossiana 18, 00184 Roma, Italy

(*First received* 1 *October* 1994 *and in final form* 16 *September* 1995)

Abstract—Most of the experimental techniques used to investigate the atmospheric turbulence give an Eulerian description of the velocity field. Nevertheless, pollutant dispersion phenomena are naturally described in the Lagrangian approach as the pollutant acts as tag of the fluid particles. The turbulence in the unstable boundary layer (UBL) of the atmosphere was simulated by means of a laboratory model and investigated from the Lagrangian point of view by use of a measuring technique (the particle tracking velocimetry) based on image analysis. The Lagrangian correlations of the horizontal and vertical velocity components were evaluated. From these, the Lagrangian integral time scales were obtained and compared with the Eulerian ones. The comparison showed that it is not possible to define a single value of the Lagrangian and Eulerian scale ratio for the whole UBL. Moreover, the data set was conditionally sampled in order to describe selectively the behaviour of upward- and downward-moving particles. Finally, assuming the horizontal homogeneity, steadiness, and frozen turbulence, the time histories of the particle locations were used to predict pollutant concentration fields, downwind continuous sources placed at any height. Copyright © 1996 Elsevier Science Ltd

Key word index: Convection, turbulence, Lagrangian statistics, integral time scale.

INTRODUCTION

The experimental investigation of the turbulence structure in the unstable boundary layer (UBL) was carried out both by means of field experiments and laboratory simulations. A large number of field experiments were performed in the last twenty years (Stull, 1988). Typically, the layer close to the ground was investigated by instrumented towers, while upper layers were probed by aircraft or tetroons. More recently, the strong technology development in the field of remote sensing gave the possibility of measuring vertical profiles of physical quantities such as velocity (SODAR), temperature (RASS), and pollutant concentration (LIDAR). The physical principles on which all these probes are based are very different; nevertheless, the data they give have at least one common property: they represent the observed quantities at fixed locations of the investigation field. This means that, historically, experimental data of atmospheric boundary layer are given in the Eulerian frame of reference. As a consequence, theoretical studies were also based mainly on the Eulerian approach because this was the only way to compare theoretical predictions with experimental data.

Nevertheless, some phenomena, occurring in the atmospheric boundary layer, are naturally described in the Lagrangian frame of reference. One of the most interesting ones is the pollutant dispersion, which is widely applied in environmental studies. As a matter of fact, pollutants act as tracers of the fluid particles, thus it is convenient to describe the behaviour of the fluid particles once they are released from the source, as they move within the field (Monin and Yaglom, 1971). Moreover, Eulerian numerical models for the prediction of pollutant dispersion (e.g. k-models) are not accurate, in particular in the UBL, where the distribution of the pollutant concentration is strongly non-Gaussian (Leuzzi, 1993). Furthermore, the inputs required for these models are parameters that cannot be generally evaluated but require an heuristic estimation depending on the case in study. Since the beginning of the 1970s a new class of models was developed (Thompson, 1971, 1987): they simulate trajectories of marked fluid particles in order to obtain ensemble average distributions of their position and velocity. Their main advantage, in comparison with Eulerian models, is their accuracy in the prediction of the concentration in proximity to the source, where high concentrations are often observed. The main constraint in their application to actual problems is that the velocity turbulence field, and Lagrangian time scale are needed as input parameters.

Attempts were made to find a relation between the Lagrangian and Eulerian time scales, both theoretical (Corrsin, 1963) and experimental (Hanna, 1981), but

the former suffers from the lack of generality while the latter relies on a small statistical base due to only insufficient field data. Finally, the vertical profiles of Eulerian and Lagrangian time scales are very different in the UBL where turbulence is neither homogeneous nor isotropic, as it will be shown later.

Some time ago, a water tank was used to investigate the convection in the planetary boundary layer (Cenedese and Querzoli, 1994). This experimental approach was not new since Willis and Deardorff (Willis and Deardorff, 1976; Deardorff and Willis, 1985) had already used similar laboratory equipment, though the measurement technique (laser Doppler anemometry) was more accurate because it was non-intrusive and non-sensitive to temperature fluctuations. Then, the same tank was used to study turbulence by a basically different technique called particle tracking velocimetry (PTV).

The basic idea of the PTV is to disperse the seeding particles homogeneously in the working fluid, tracking them during their motion, and evaluating the history of velocity along the trajectory of each particle by means of the image analysis. The resulting description of the velocity field is intrinsically Lagrangian. From these data, Lagrangian statistics are evaluated and the integral time scale is compared with the Eulerian one. The acquired data set was then conditionally sampled to obtain a selective description of the two main classes of phenomena occurring in the UBL: hot updrafts and cold downdrafts. Finally, the conditional sampling was used in a different way in order to simulate the pollutant dispersion from a "virtual" source located at any height within the field. The latter result is very useful for the validation of Lagrangian particle models because the concentration fields (i.e. the output of the models) were evaluated from the same data set used for the evaluation of velocity field and Lagrangian statistics (i.e. the input of the models).

EXPERIMENTAL SET-UP

(a) *The laboratory model*

The UBL is simulated by a convection chamber filled with water and heated from below. Its horizontal dimensions are 41 cm × 41 cm and side walls are of 0.80-cm thick glass sufficient to avoid meaningful heat losses. In order to enhance heat exchange, the lower surface is made up of an aluminium plate 0.80 cm thick. Under the plate, a heat exchanger is placed in a shallow chamber (2.50 cm deep) filled with water, to obtain a homogeneous heating of the lower surface. The free surface of the water is insulated by a polystyrene slab to avoid the cooling due to evaporation.

During each experiment, the tank was at first filled with 10 cm of ambient temperature water, then a second layer of hot water (20°C higher than the first one) was slowly stratified from above to obtain a thermal stratification corresponding to the capping inversion (CI) present in the atmosphere. After about half an hour, a constant lapse rate was observed from 7 to 13 cm. The heating was then applied to the lower surface simulating the effect of the solar radiation on the soil. A 240 s time interval was left for the turbulent convection to be completely developed, before the acquisition was begun (for a more detailed description of the tank and of experimental procedures see Cenedese and Querzoli, 1994). The development of the convection after this time delay was confirmed by visualizations and measurement of the temperature statistics performed in preliminary experiments.

(b) *The particle tracking velocimetry*

The image analysis system is sketched in Fig. 1: a 3 CCD video camera was connected to a frame grabber (512 pixels × 512 pixels in resolution) through an S-VHS videorecorder and an animation controller. A personal computer connected both to the frame grabber and animation controller, controlled the entire flow of operations. The functions of the animation controller were to insert a frame code during recording and to operate the videorecorder automatically by means of the personal computer.

The water was seeded by non-buoyant particles, 200 μm in diameter, and it was illuminated by a 1000 W arc lamp. In order to obtain an almost parallel light beam illuminating the tank, the lamp was placed as far as 2.5 m from the test section. The measuring volume was defined by the intersection of the illuminated volume and the area framed by the video camera. In the experiment it was 10 cm high, 12.5 cm wide and 5.0 cm deep.

The acquiring procedure may be ideally divided into four steps (Fig. 2): at first, images are recorded on tape, then the images of particles and their locations are identified and next, the particle tracking itself is performed and finally the velocity field is evaluated. The technique is correct under the assumption that the seeding particles behave exactly as the fluid particles. This means that they have to be small in comparison with the spatial scale of the convective phenomena and their density should not be significantly different from that of water. The dimension of particles is trivially much smaller than the scale of the structures under investigation, while the evidence that the latter requirement is met was given by the fact that particles remained in suspension in still water for about 1 h during the preparation of the experiment.

Recording images: During the acquisition, the animation controller inserts a frame code so that random access to each image on tape is possible. This is the only step of processing that was performed on-line.

Recognition of particles: The acquired frames contain bright images of the particles (hereafter called spots) on a dark background. Frames are digitised by the frame grabber and given a threshold. As a result, background pixel intensity is set to zero, whereas pixels belonging to a bright area are set to one. Then the spots are recognised by identifying the sets of connected lighted pixels, and their centroid locations are calculated.

Particle tracking: The result of the previous procedure is a list of particle locations together with the information about the time at which they were acquired. Trajectories are recognised by examining the spot list and looking for time-ordered series of spots that fulfil the following rules:

(i) Maximum distance between two successive spots must be less than a given value D.

(ii) Maximum difference between two successive displacements of a particle must be less than a given value e.

(iii) A trajectory must consist of at least three spots.

The parameters D and e support a physical interpretation: D represents the maximum velocity assumed for the field, whereas e represents the maximum acceleration. Tuning of these parameters is the basic point of PTV: if the choice is too restrictive, high-speed particles are not tracked. On the other hand, if the parameters are too large, a significant number of errors occur during the trajectory recognition.

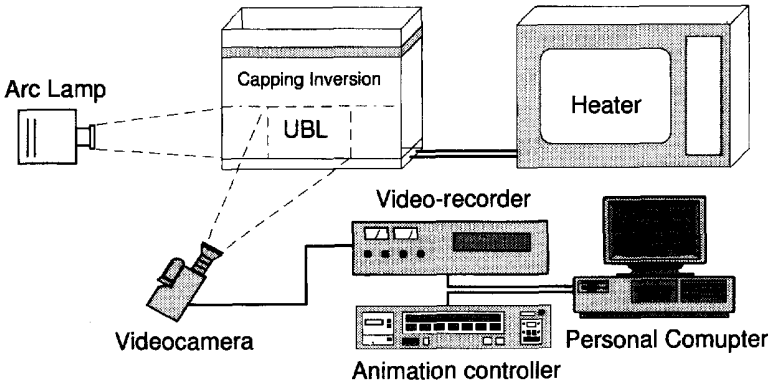

Fig. 1. Scheme of the image analysis system.

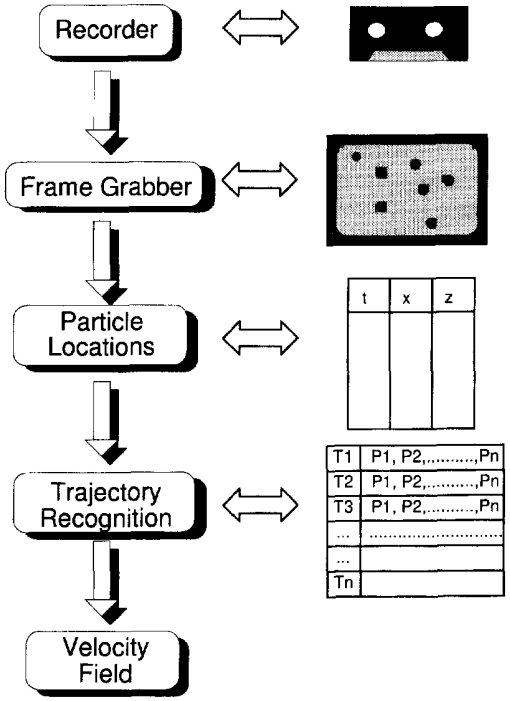

Fig. 2. Flow chart of the image processing.

Evaluation of the velocity field: Finally, particle displacements are divided by the time interval between two frames, resulting in a Lagrangian description of the velocity field.

RESULTS AND DISCUSSION

Data set and scaling

The data set was obtained from 20 runs of the same experiment. In any given run, the recording began 240 s after the heating had been applied; this instant was considered the origin of the time. Since the sampling rate of the videorecorder was 25 Hz, too high for the particles to move meaningfully from one frame to the next, only one in every 10 frames was digitised and examined. The resulting sampling frequency was 2.5 Hz and spot locations were evaluated 2500 times per run, reaching a total acquisition period of 1000 s. Optimal values of tracking parameters were determined, after a set of tests, by comparing the resulting probability distribution of the velocity with that obtained from laser Doppler measurements (Cenedese and Querzoli, 1994). Typical values of these parameters were: $D = 50$ pixels, $e = 10$ pixels.

Results are presented in non-dimensional form by using the similarity proposed by Deardorff (1970).

The convective scaling assumes the mechanical production of turbulence kinetic energy to be negligible in comparison with buoyant production. Under this assumption, the scaling parameters are:

$$\text{convective velocity:} \quad w_* = \sqrt[3]{g \cdot \alpha \cdot q_s \cdot z_i} \tag{1}$$

$$\text{height of UBL:} \quad z_i \tag{2}$$

$$\text{convective temperature:} \quad \vartheta_* = \frac{q_s}{w_*} \tag{3}$$

$$\text{convective time:} \quad t_* = \frac{z_i}{w_*} \tag{4}$$

where g is the acceleration of gravity, α is the thermal expansion coefficient, and q_s is the surface kinematic heat flux (see Cenedese and Querzoli, 1994, for typical values of parameters in tank and atmosphere). It should be noted that the phenomena occurring in the UBL are not steady: its height and mean temperature increase with time. Thus the scaling parameters are functions of time. In order to compare data not acquired simultaneously, quasi-steadiness has to be assumed. This means that the system changes through a succession of steady states. Hence, after normalisation, it can be considered time independent.

Lagrangian reference frame

Let $\mathbf{X}$ indicate the location of a fluid particle with respect to a fixed frame of reference and let $\mathbf{x}$ be the location of the same particle at a reference time t_0, i.e. $\mathbf{x} = \mathbf{X}(\mathbf{x}, t_0)$. If $\mathbf{x}$ is kept constant, $\mathbf{X}(\mathbf{x}, t)|_{\mathbf{x}}$ indicates the trajectory of the fluid particle identified by its location at the reference time. $\mathbf{x}$ can be regarded as a system of curvilinear coordinates that deforms with fluid. The Lagrangian velocity field is given by

$$\mathbf{V}(\mathbf{x}, t) = \left.\frac{\partial \mathbf{X}(\mathbf{x}, t)}{\partial t}\right|_{\mathbf{x}} \tag{5}$$

and it is related to the Eulerian velocity u by the formula

$$\mathbf{V}(\mathbf{x}, t) = \mathbf{u}[\mathbf{X}(\mathbf{x}, t), t]. \tag{6}$$

In its general formulation, the Lagrangian auto-correlation $R_i(\mathbf{x}_1, t_1, \mathbf{x}_2, t_2)$, is defined as the average product of velocity $V_i(\mathbf{x}, t_1)$ and $V_i(\mathbf{x}, t_2)$ of all particles that at time t_1 are at $\mathbf{x}_1$ and at time t_2 are at $\mathbf{x}_2$ (Monin and Yaglom, 1971). Such a formulation is more suitable in a non-homogeneous and non-steady field. Nevertheless, it can be simplified by assuming the phenomenon to be quasi-steady and homogeneous on the horizontal plane. From the first assumption the auto-correlation function is not dependent on the initial time t_1 but only on the time interval $\tau = t_2 - t_1$ and from the latter results that it is spatially dependent on the vertical abscissa only.

Lagrangian auto-correlations

In Fig. 3, the auto-correlation coefficient, $r_w(\tau, z) = R_w(\tau, z)/R_w(0, z)$, of the vertical and horizontal velocity component, is plotted as a function of the dimensionless time lag at three heights of UBL (solid lines). It may be noted that the vertical velocity auto-correlations (solid lines) cross the axis after a time lag contained in the interval [0.5; 1.0], and exhibits a minimum between 1.0 and 1.5. This is due to the large convective structures that dominate the UBL. It typically happens that a particle that is ascending in a hot thermal, after a period a little longer than t_*, descends in a cold downdraft. At longer time lags the oscillation continues but its amplitude tends to vanish because the coherent structures of the UBL are not stable for long enough and the memory of their presence is lost after about 2.3 ~ 3.0 times t_*. Although the convection is characterised by an irregular and unsteady pattern, most of the structures are coherent all over the height of the UBL. Nevertheless, they are often pushed aside by other structures arising in their neighbourhood, modifying the shape of convective cells, so the auto-correlation coefficient of the horizontal velocity component r_u (Fig. 3, dashed lines) does not exhibit a negative minimum and, whatever the height, it does not have a well-defined intersection with the

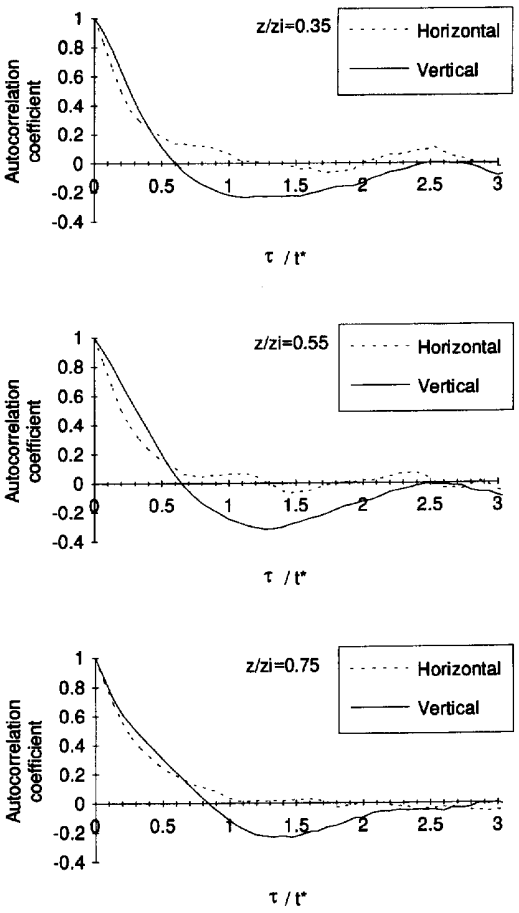

Fig. 3. Lagrangian auto-correlation of the horizontal (dashed lines) and vertical (solid lines) components of velocity at three different levels (z/z_i = 0.35, 0.55, 0.75).

time axis. The auto-correlation drops to very small values as the time lag is greater than t_*.

Lagrangian vs Eulerian time scale

The Lagrangian integral time scale $T_{\mathscr{L}}$ is a parameter describing how long a fluid parcel "remembers" its past. In other terms, the larger it is, the longer a particle will be affected by what happens at present. The Lagrangian time scale relative to the ith component of velocity is generally obtained by integration of the corresponding auto-correlation coefficient:

$$T_{\mathscr{L},i}(z) = \frac{1}{t_*} \int_0^\infty r_i(\tau, z)\, \mathrm{d}\tau. \tag{7}$$

This definition is, in point of fact, not applicable since auto-correlations obtained from experimental data do not approach zero at the greater available time lag. Therefore, the so-called $1/e$ scale, T_L, was evaluated, i.e. the time lag at which the auto-correlation coefficient drops to $1/e$. The latter definition corresponds to the former if the auto-correlation function is exponential:

$$r(\tau, z) = e^{-\tau/T_{\mathscr{L}}} \cdot f(z). \tag{8}$$

Hanna (1981) stated that, under reasonable assumptions, Lagrangian (T_L) and Eulerian (T_E) time scales are simply related, and proposed some values of the coefficient $\beta = T_L/T_E$. As a matter of fact, in the case of homogeneous and isotropic turbulence, some considerations about the time scales ratio can be made (Corrsin, 1963), but in the UBL, where large, non-isotropic structures (order of z_i) drive the mixing process, a single value of β is not observed. The reason is that the Eulerian scale is computed from the time history of the velocity at a given location. This means it is more related to the *permanence* of a structure at the measuring point rather than to its dimension or lifetime. On the contrary, the Lagrangian one is more influenced by the latter features.

In Fig. 4 the non-dimensional vertical profiles of the Lagrangian and Eulerian time scales of the horizontal velocity are drawn. The Eulerian time scales were evaluated from measurements carried out during the first series of experiments (Cenedese *et al.*, 1992). Focusing on the Lagrangian one, the UBL can be ideally divided into three zones. Two of them ($0 \leqslant z/z_i \leqslant 0.3$ and $0.9 \leqslant z/z_i \leqslant 1.2$), near the upper and lower boundaries, are characterised by a horizontal main motion. In these zones, two relative maxima are observed: the one located near the top of the UBL has a larger amplitude because, close to the CI, particles move typically slower than in proximity to the hot surface where the buoyancy force acts. On the contrary, the third zone, located at middle height, is characterised by a vertical main motion and by small horizontal time scales. The Eulerian scale also exhibits a similar behaviour, but more smoothly and with maxima in a lower position. Actually, the Eulerian time scale can be considered almost constant in the bulk of the UBL due to the strong mixing. At the top of the UBL, where large structures are often present, but they move each other about, the Eulerian scale is much smaller than the Lagrangian one.

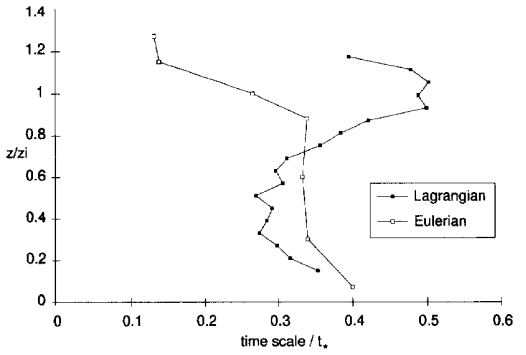

Fig. 4. Non-dimensional profiles of the Lagrangian and Eulerian integral time scales of the horizontal velocity component.

Non-dimensional Eulerian and Lagrangian time scales of the vertical velocity component are shown in Fig. 5. The Eulerian scale slightly decreases in the middle of the UBL, whereas it decreases in proximity to the CI, where the thermal stability dampers the large scale motions and generates, fast, vertical oscillations. It also diminishes at the lower heights where the surface cuts off the large structures. The overall behaviour of the vertical velocity Lagrangian scale is very different from that of the horizontal component. It increases from one third of the UBL height, up where the effect of the thermal stability is predominant, then it drops. The explanation for the opposite slope of the curves in the middle part of the UBL can be found in the mechanism of growth of the convective cells: small structures are generated near the surface and merge together as they rise through the layer. As a consequence, the typical dimension of the structures with height (as well as the Lagrangian scale), whereas their permanence time at a location diminish (and the Eulerian scale too) since they have lateral interactions and are pushed down by the thermal stability of the CI.

The Lagrangian scale drops at higher values of non-dimensional height in respect to the Eulerian one because Eulerian scale takes into account only the behaviour of the fluid in the neighbourhood of the location where it is calculated, while the Lagrangian one is based on tracking fluid particles. Thus it is also affected by non-homogeneity of the field at large distance. For instance, the Lagrangian scale evaluated in the proximity of the CI is affected both by particles remaining in its neighbourhood (with a small scale) and by those traversing the entire UBL (with large scale).

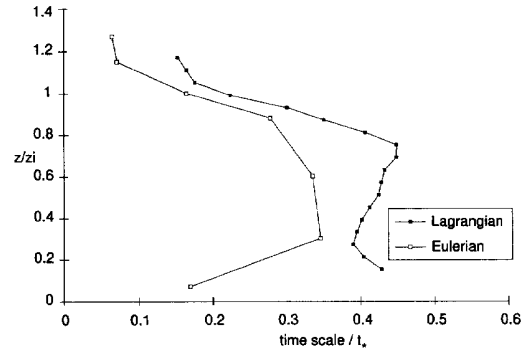

Fig. 5. Non-dimensional Eulerian and Lagrangian $1/e$ time scale of the vertical velocity as functions of non-dimensional height.

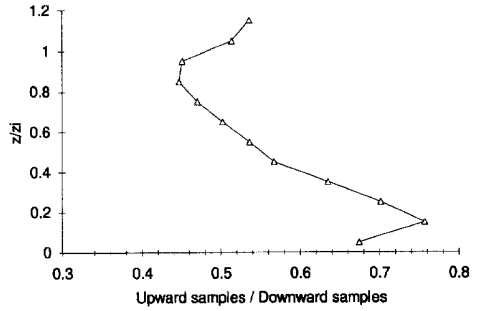

Fig. 6. Ratio of upward to downward moving trajectories.

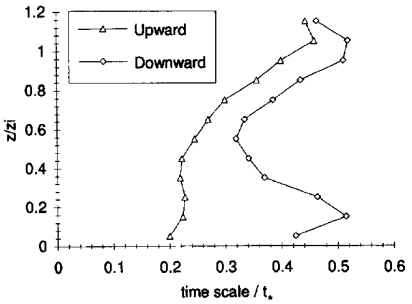

Fig. 7. Vertical profile of the conditioned Lagrangian time scales of the horizontal velocity. Triangles indicate the time scale of the trajectories whose first velocity is upwards and parallelograms indicate time scale of trajectories with negative initial vertical velocity.

Conditional sampling

The idea that, in a flow dominated by large structures (order of z_i), Lagrangian statistics are influenced by non-uniformity of the field, suggests the definition of a further class of statistics. Let us consider, for example, a particle that, at the initial time, is located close to the lower surface, two cases may occur:

(i) the particle is going up: presumably it arises through the whole height of UBL before losing its correlation and it has a large time scale;

(ii) the particle is going down: soon it reaches the surface and it is forced to change direction, therefore its scale is necessarily small.

Both cases give their contribution to the evaluation of the same value of the Lagrangian statistics in spite of the different phenomena they represent. In general, whatever the starting height, the behaviour of the upward and downward moving particles is completely different.

In order to point out this difference, the set of acquired trajectories was divided into two subsets: one is the set of the trajectories whose first velocity is positive, the other includes the trajectories with negative initial velocity. Then, Lagrangian auto-correlations and time scales were evaluated separately for the two sets.

The number of upward over that of downward-moving particles is shown in Fig. 6. It is always less than 1 because cold downdrafts are more probable than hot thermals, and it increases from the lower surface, where the maximum number of uprising particles is found, to the top of the UBL.

Conditioned Lagrangian time scales

In Fig. 7, the upward and downward time scales of the horizontal velocity components are plotted as functions of non-dimensional height. The largest scale of the downward-moving particle occurs near the surface and at the top of the UBL because, in these regions, the main motion is horizontal and downdrafts are slow. As a consequence, they take a long time to change their horizontal velocity orientation and to lose their correlation.

Particles associated with uprising thermals are typically characterised by sudden accelerations after which they quickly go through the whole UBL until they reach the CI. This kind of behaviour is characterised by a low horizontal velocity; thus they often reverse the velocity orientation and lose the correlation. As a result, the upward time scale is always shorter than the downward one. Moreover, it increases with height because, during their rise through the UBL, small structures merge together into large structures (Hunt *et al.*, 1988) while the vertical velocity drops, letting particles be correlated for longer time lags.

Figure 8 shows the conditioned time scales of the vertical velocity as measured in the tank. Particles of thermals, originally near the surface can rise for a long time before they find the top of the UBL, but descend for only a short time. The opposite happens for particles starting near the CI. Therefore, the upward scale constantly decreases with height whereas an opposite slope is observed for the downward scale. As above, the upward scale is, in general, smaller than the downward one because the hot thermals generate larger vertical velocity than the downdrafts, hence a particle typically takes less time to go from the bottom to the top of the UBL than vice versa.

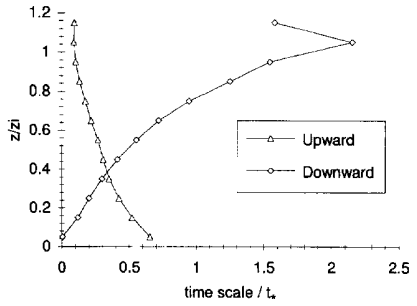

Fig. 8. Vertical profile of the conditioned Lagrangian time scales of the vertical velocity. Triangles indicate the time scale of the trajectories whose first velocity is upwards and parallelograms indicate time scale of trajectories with negative initial vertical velocity.

Pollutant dispersion

The raw data obtained by PTV describe the displacement of all the seeding particles tracked during acquisition. By analysing this data set, it is possible to evaluate the concentration field of pollutants instantaneously released from a point source placed within the UBL. The conditional sampling was used again to calculate the particle displacement statistics equivalent to the one produced by a source physically placed in the tank. The data set included only the trajectories of particles that started from the height of the simulated source. Then, following the Willis and Deardorff (1974) approach, through the frozen turbulence hypothesis, a mean wind was simulated. The time evolution of the concentration field was transformed into a space evolution downwind to a continuous source. This method has the advantage that it is non-intrusive, i.e. no physical devices have to be placed in the tank during measurements to actually release the pollutant. Thus the velocity field is not perturbed and it is possible to simulate "virtual" sources placed at any height.

Let z_S indicate the height of the simulated source and Δz_S a tolerance parameter: particles are tracked until one of them is found at height $z_S \pm \Delta z_S/2$, then it is considered released from the virtual source. Let $P_0(x_0, z_S)$ and t_0 indicate, respectively, location and time of that particle at the instant of release. The statistics of displacement relative to P_0 were evaluated assuming t_0 to be the time origin, for all the particles intersecting the source height. In a more proper formulation, the probability $p(y - y_0, z|t - t_0, z_S)$ was evaluated that a particle is at height z and has a horizontal displacement $y - y_0$ after a time $t - t_0$ since it was at height z_S. The concentration field due to an instantaneous point source is

$$C(t - t_0, y - y_0, z) = N(t - t_0)\, p(y - y_0, z|t - t_0, z_S) \tag{9}$$

where $N(t - t_0)$ is the number of released particles present in the field after a time interval $(t - t_0)$. Integrating equation (9) along y, with the time interval after release, $(t - t_0)$, denoted by τ,

$$c(\tau, z) = N(\tau)\, p(z \mid \tau, z_S). \tag{10}$$

The integrated concentration was finally normalised by the uniform concentration

$$c_0(\tau) = \frac{N(\tau)}{z_i} \tag{11}$$

so that the non-dimensional concentration field depends neither on the actual number of trajectories intersecting $z = z_S$ nor on their length.

Since a thin layer close to the lower surface is not framed by the video camera, if a particle reaches it, its trajectory is interrupted. Thus the concentrations given in the following correspond to a lower boundary condition of total absorption.

As mentioned before, assuming frozen turbulence, the non-dimensional time $T = t/t_*$ was transformed in non-dimensional downwind length X_d: the frozen turbulence hypothesis furnishes:

$$t = \frac{x}{U} \tag{12}$$

where x is the downwind length and U the simulated mean wind, then

$$T = \frac{t}{t_*} = \frac{x}{U}\, t_* = X_d. \tag{13}$$

Three surface heights were considered ($z_S/z_i = 0.25$, 0.50, 0.75) and the contour plots of the normalised concentration fields are presented in Figs 9–11, as functions of X_d and z/z_i; the mean height of the particles is plotted in Fig. 12.

When the source is near the ground ($z_S/z_i = 0.25$), due to the negative mode of the vertical velocity probability distribution, the maximum of concentration descends, reaching the surface at $X_d \cong 0.3$. Far from the source, the maximum rises to $z/z_i = 0.5$, where the mean particle height is found as well. Similarly, when the source is placed at half the UBL height, the highest concentration descends, but it takes a little longer to reach the surface ($X_d \cong 0.7$). Moreover, the ground concentration exhibits a minimum at about $X_d \cong 1.4$. Finally, when the source is located near the top of the UBL ($z_S/z_i = 0.75$), concentration at the surface is less because the plume is widely spread before the maximum approaches the ground. In all cases, the pollutant is trapped within the UBL by the overlaying CI, and concentration drops to lower values as height increases over z_i. Furthermore, fluctuations and some increased concentration values observed at a great distance from the source are due to the diminishing number of trajectories long enough to be taken into account; thus the number of samples averaged is smaller.

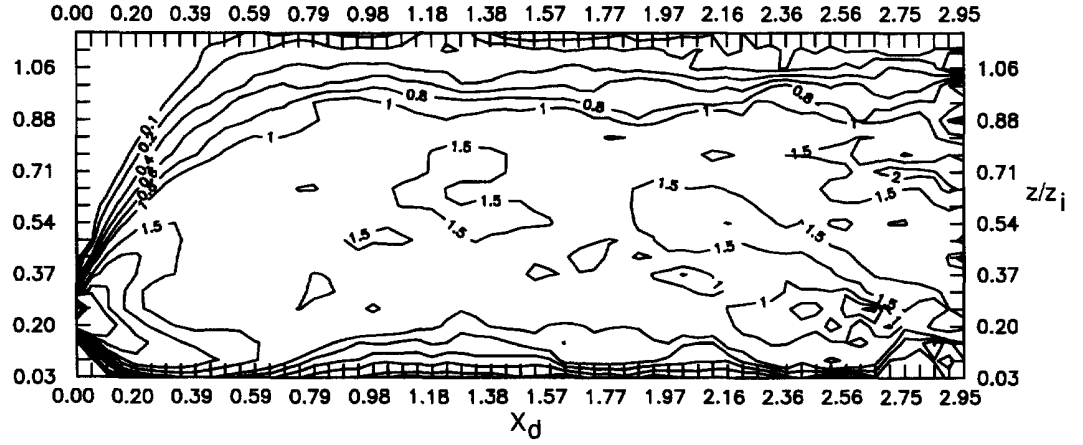

Fig. 9. Contour plot of the non-dimensional concentration field for a source placed at $z_S/z_i = 0.25$.

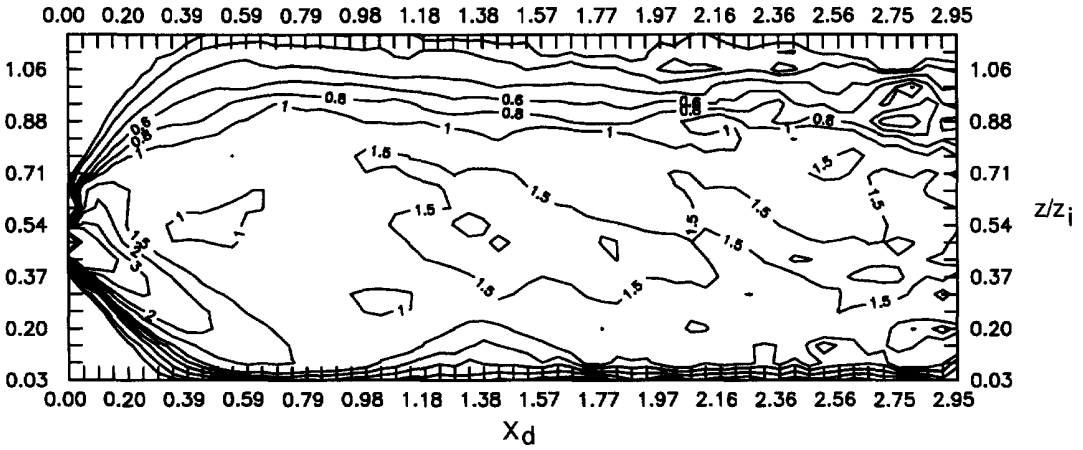

Fig. 10. Contour plot of the non-dimensional concentration field for a source placed at $z_S/z_i = 0.50$.

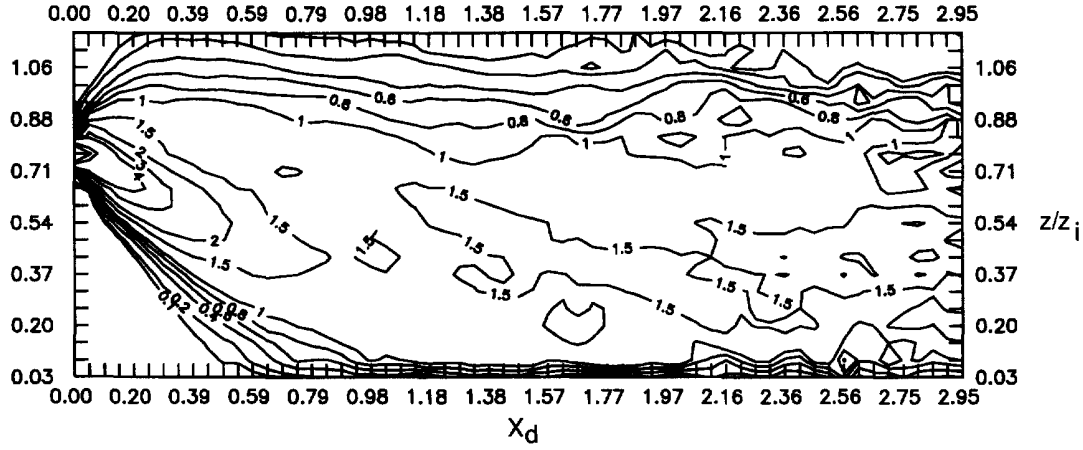

Fig. 11. Contour plots of the non-dimensional concentration field for a source placed at $z_S/z_i = 0.75$.

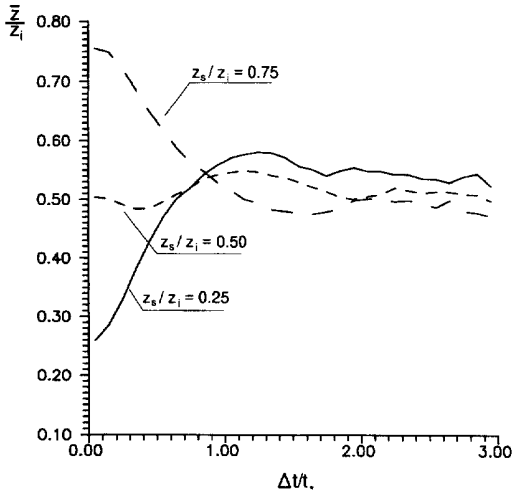

Fig. 12. Mean height of particles dispersed from the virtual sources at height $z_s/z_i = 0.25, 0.50, 0.75$.

CONCLUSIONS

The PTV permitted the direct evaluation of the Lagrangian characteristics of the UBL turbulence. It was observed that, since the field is neither homogeneous nor isotropic, it is not possible to identify a single value of the Lagrangian integral time scale representative of the whole UBL. Moreover, the comparison with the Eulerian time scale showed that the Lagrangian and Eulerian scale ratio is not constant but depends on height.

The description of UBL turbulence in terms of ascending and descending particles pointed out that the particles belonging to hot updrafts behave differently from those belonging to the cold downdrafts. The complex mixing process is well described as the result of the superimposition of the two basic processes. Finally, the prediction of pollutant concentration fields is an effective comparison test for Lagrangian numerical models, because the concentration field and the integral time scale are experimentally determined from the same data set in well-known initial and boundary conditions.

Acknowledgements—I am indebted to A. Cenedese for providing the incentive and facilities to study atmospheric convection. I thank G. Leuzzi for a number of helpful discussions on theoretical problems involved in this study and A. Fiorentino for his valuable help.

REFERENCES

Cenedese A. and Querzoli G. (1994) A laboratory model of turbulent convection in the atmospheric boundary layer. *Atmospheric Environment* **28,** 1901–1913.

Cenedese A., Franceschi M. A. and Querzoli G. (1992) A laboratory simulation of dispersion phenomena in the atmospheric convective boundary layer. In *Proc. 2nd Minsk Int. Heat and Mass Transfer Forum*, Minsk.

Corrsin S. (1963) Estimates of the relation between Eulerian and Lagrangian scales in large Reynolds number turbulence. *J. atmos. Sci.* **20,** 115–119.

Deardorff J. W. (1970) Convective velocity and temperature scales for the unstable planetary boundary layer and for Raileigh convection. *J. atmos. Sci.* **27,** 1211–1213.

Deardorff J. W. and Willis G. E. (1985) Further results from a laboratory model of the convective planetary boundary layer. *Boundary-Layer Met.* **32,** 205–236.

Hanna S. R. (1981) Lagrangian and Eulerian time scale relations in the day-time boundary layer. *J. appl. Met.* **20,** 242–249.

Hunt C. R., Kaimal J. C. and Gaynor J. E. (1988) Eddy structure in the convective boundary layer—new measurements and new concepts, *Q. Jl R. Met. Soc.* **114,** 827–860.

Leuzzi G. (1993) Modelli per il Calcolo della Dispersione di Inquinanti, Doctoral Thesis, Department of Mechanics and Aeronautics, University of Rome, pp. 155

Monin A. S. and Yaglom A. M. (1971) *Statistical Fluid Mechanics*. MIT Press, Cambridge.

Stull R. B. (1988) *An Introduction to Boundary Layer Meterology*, p. 666. Kluwer Academic Publishers, Dordrecht.

Thompson R. (1971) Numerical calculation of turbulent diffusion. *Q. Jl R. Met. Soc.* **97,** 93–98.

Thomson D. J. (1987) Criteria for the selection of stochastic models of particles trajectories in turbulent flows. **180,** 529–556.

Willis G. E. and Deardorff J. W. (1974) A laboratory model of the unstable planetary boundary layer. *J. atmos. Sci.* **31,** 1297–1307.

Willis G. E. and Deardroff J. W. (1976) A laboratory model of diffusion into the convective planetary boundary layer. *Q. Jl R. Met. Soc.* **102,** 427–445.